Title: Data-driven metasurface discovery

Authors:

Jiaqi Jiang[1], David Sell[2], Stephan Hoyer[3], Jason Hickey[3], Jianji Yang[1], and Jonathan A. Fan[1]

Affiliations:

[1]Department of Electrical Engineering, Stanford University, Stanford, CA, USA.

[2]Department of Applied Physics, Stanford University, Stanford, CA, USA.

[3]Google AI Applied Science, Mountain View, CA, USA.

Abstract:

A long-standing challenge with metasurface design is identifying computationally efficient methods that produce high performance devices. Design methods based on iterative optimization push the performance limits of metasurfaces, but they require extensive computational resources that limit their implementation to small numbers of microscale devices. We show that generative neural networks can learn from a small set of topology-optimized metasurfaces to produce large numbers of high-efficiency, topologically-complex metasurfaces operating across a large parameter space. This approach enables considerable savings in computation cost compared to brute force optimization. As a model system, we employ conditional generative adversarial networks to design highly-efficient metagratings over a broad range of deflection angles and operating wavelengths. Generated device designs can be further locally optimized and serve as additional training data for network refinement. Our design concept utilizes a relatively small initial training set of just a few hundred devices, and it serves as a more general blueprint for the AI-based analysis of physical systems where access to large datasets is limited. We envision that such data-driven design tools can be broadly utilized in other domains of optics, acoustics, mechanics, and electronics.

Main Text

Metasurfaces are foundational devices for wavefront engineering because they have electromagnetic properties that are tailored by subwavelength-scale structuring *(1-3)*. Metasurfaces can focus and steer an incident wave *(4)* and manipulate its polarization *(5)* in nearly arbitrary ways, surpassing the limits set by conventional optics. They can also shape and filter spectral features, which has practical applications in sensing *(6)*. Metasurfaces have been implemented in frameworks as diverse as holography *(7)* and transformation optics *(8)*, and they can be used to perform mathematical operations with light *(9)*.

Conventional metasurfaces utilize discrete phased array elements, such as plasmonic antennas *(10)*, nanowaveguides *(11, 12)*, and Mie-resonant nanostructures *(13)*. These devices produce high efficiency responses when designed for modest deflection angles and single functions. However, when designed for more advanced capabilities, they suffer from reduced efficiencies due to their restrictive design space. Iterative topology optimization, including adjoint-based *(14)* and objective-first *(15)* methods, is an alternative design approach that can extend the capabilities of metasurfaces beyond those utilizing phased array elements. Devices based on this concept have non-intuitive, freeform layouts, and they can support high efficiency, large angle, multi-wavelength operation *(16-20)*. However, the design process is computationally intensive and requires many simulations per device, limiting its implementation to small numbers of microscale devices.

In this Article, we show that conditional generative adversarial networks (GANs) *(21, 22)* can serve as an effective and computationally efficient tool to produce large numbers of high performance metasurfaces with advanced functionalities across a range of operating parameters. As a model system, we utilize a conditional GAN to generate silicon metagratings *(23,24)*, which are periodic metasurfaces designed to deflect electromagnetic waves to a desired diffraction order (Fig. 1a). Our initial training set is small and consists of 600 high-resolution images of high efficiency, topology-optimized devices. After training, the GAN can generate thousands of high performance metagratings operating across a broad range of wavelengths and angles. Compared to devices designed using only iterative optimization, our use of the conditional GAN provides clear advantages in computational efficiency in the limit where we want to produce thousands of high performance devices. This study shows that neural networks are capable of learning features in topologically complex metasurfaces, and that they have the potential to produce high performance, large area devices with tractable computational resources.

Our machine learning approach is qualitatively different from those based on feedforward neural networks, which attempt to explicitly learn the relationship between device geometry and electromagnetic response. In prior studies, neural networks were applied to the inverse design of relatively simple shapes, described by a small number of geometric parameters *(25-29)*. These studies successfully demonstrated the potential of deep neural networks for electromagnetics design. However, they required tens of thousands of training data points and are limited to the design of simple geometries, making the scaling of these concepts to complicated shapes extremely data intensive. With conditional GANs, which are deep generative models, we directly sample the space of high efficiency designs without the need to accurately predict the performance of every device along an optimization trajectory. The algorithms focus on learning important topological features harvested from high-performance metasurfaces, rather than attempting to predict the behavior of every possible device, most of which are very far from optimal. In this manner, these

networks produce high efficiency, topologically-intricate metasurfaces with substantially less training data.

Our starting point is the production of a high-quality training set consisting of high-resolution images of topology-optimized metagratings (Fig. 1a and Fig. 1b). Each device is 325 nm thick and designed to operate at a wavelength between 800 nm to 1000 nm, in increments of 20 nm, and at an angle between 55 and 65 degrees, in increments of 5 degrees. For each wavelength and angle pair, we generate a distribution of devices with a range of efficiencies, using different random dielectric starting layouts. We then keep 45 of the high efficiency "above threshold" devices, which we define to be those operating in the top 40th percentile of the efficiency distribution (see Fig. S4 for distribution examples).

These data are used to train our conditional GAN, which consists of two networks, a generator and a discriminator (Fig. 1c). The generator is trained to produce images of new devices. Its inputs are the metagrating deflection angle, operating wavelength, and an array of normally-distributed random numbers, which provides diversity to the generated device layouts. The discriminator is trained to distinguish between actual devices from the training set and those from the generator. The training process can be described as a two-player game in which the generator tries to fool the discriminator by generating real-looking devices, while the discriminator tries to identify and reject generated devices from a pool of generated and real devices. In this manner, the discriminator serves as a simulator that evaluates the performance of the generator and learns based on this information. Upon training completion, the generator will have learned the underlying topological features from optimized metagratings, and it will be able to produce new, topologically complex devices for a desired deflection angle and wavelength input. The diversity of devices produced by the generator reflect the use of a random noise input in our probabilistic model. Details pertaining to the network structure and training process are in the Supplementary Section.

To illustrate the performance of our conditional GAN, we use our trained generator to produce 5000 different layouts of devices operating at a 70 degree deflection angle and a 1200 nm wavelength. This operating wavelength is red-shifted beyond those of all devices used for training. We calculate device efficiencies using a rigorous coupled-wave analysis solver *(31)*, and the distribution of efficiencies is plotted as a histogram in Fig. 2a. The histogram of device efficiencies produced from the conditional GAN shows a broad distribution. Notably, there exist devices in the distribution with efficiencies over 60% and as high as 62%. The presence of these devices indicates that our conditional GAN is able to learn and generalize features from the metasurfaces in the training set.

To benchmark these device metrics, we characterize 5000 random binary patterns with feature sizes similar to those in our training set (Fig. S1a). The efficiency histogram of these devices is also plotted in Fig. 2a and shows that the best device is only 30% efficient, indicating that randomly-generated patterns all exhibit poor efficiencies. We also evaluate and plot the deflection efficiencies of devices in the training set that have been geometrically stretched, such that they diffract 1200 nm light to 70 degrees. The efficiency histogram of these devices is also plotted in Fig. 2a and displays a maximum efficiency of only 53%.

The ability for the generator to extrapolate the topological features of high efficiency devices is due in part to its ability to generate a large number of devices with diverse geometric features (Fig. S3). Device generation, even for thousands of devices, is computationally efficient and takes only a few seconds using a standard computer processing unit. In the example above, the number of

devices produced and tested from the GAN generator is nearly an order of magnitude larger than the entire training set.

The high efficiency devices produced by the conditional GAN can be further refined with iterative topology optimization. This additional refinement serves multiple purposes. First, it further improves the device efficiencies. Second, it incorporates robustness to fabrication imperfections into the metagrating designs, which makes experimentally fabricated devices more tolerant to processing defects *(23)*. Third, it enforces other experimental constraints, such as grid snapping or minimum feature size. Relatively few iterations of topology optimization are required at this stage because the devices from the conditional GAN are already highly efficient and near a local optimum in the design space.

With this approach, we apply 30 iterations of adjoint-based topology optimization to the 50 highest efficiency GAN-generated devices from Fig. 2a. With topology refinement, devices are optimized to be robust to geometric erosion and dilation. The final device efficiency distributions are plotted in Fig. 2b. Interestingly, some of the devices have efficiencies that lower after topology optimization. The reason is that these devices from the generator were not initially robust, and their efficiencies were penalized as the optimizer enforced robustness constraints into the designs. The highest performance device has an efficiency of 86%. Results of this analysis for other wavelengths and deflection angles are summarized in Fig. S2. Compared to the efficiency distribution of devices topology-optimized from scratch (Fig. S4, fourth column), this highest performance device operates in the top 40^{th} percentile in efficiency. A plot of device efficiency over the course of iterative optimization for this metagrating is shown in Fig. S5.

Our strategy to design robust, high-efficiency metagratings with the GAN generator and iterative optimizer can apply to a broad range of desired deflection angles and wavelengths. With the same training data from before, we design robust metagratings with operating wavelengths ranging from 500 nm and 1300 nm, in increments of 50 nm, and angles ranging from 35 and 85 degrees, in increments of 5 degrees. 5000 devices are initially generated and characterized for each angle and wavelength, and topology refinement is performed on the 50 most efficient devices. Fig. 3a shows the device efficiencies from the generator, where the efficiencies of the highest performing devices for a given angle and wavelength are presented. Most of the generated devices have efficiencies over 65%, and within and near the parameter space specified by the training set (yellow box), the generated devices have efficiencies over 75%.

Representative images of high efficiency metagratings from the generator are shown in Fig. 3b. We find that at shorter wavelengths, the metagratings generally comprise spatially distributed dielectric features. As the wavelengths get longer, the devices exhibit more consolidated distributions of dielectric material with fewer voids. These variations in topology are qualitatively similar to those featured in the training set (Fig. 1b). Furthermore, these trends in topology clearly extend to devices operating at wavelengths beyond those used in the training set. Additional images of devices from GAN generator are shown in Fig. S6.

The device efficiencies of the best devices after topology refinement are presented in Fig. 3c. We see that nearly all the metagratings with wavelengths in the 600–1300 nm range and angles in the 35–75 degree range have efficiencies near or over 80%. Not all the devices produced with our method exhibit high efficiencies, as Fig. 3c shows clear drop-offs in efficiencies for devices designed for shorter wavelengths and ultra-large deflection angles. One source for this observed drop-off is that these devices are in a parameter space that requires topologically distinctive

features that could not be generalized from the training set. As such, the conditional GAN is unable to learn the proper patterns required to generate high performance devices. We also note that there are device operating regimes for which high efficiency beam deflection is not physically possible with 325 nm-thick silicon metagratings. For example, device efficiency will drop off as the operating wavelength becomes substantially larger than the device thickness *(32)* and when the deflection angle becomes exceedingly large (Fig. S4, fifth column).

Our use of the conditional GAN provides clear advantages in computational efficiency compared to brute force topology optimization, in the limit where we want to produce many thousands of high performance devices, including many devices for each wavelength and angle pair. The identification of large numbers of high performance devices is important because it enables the use of statistical, large data analyses to deepen our understanding of the high-dimensional phase space for metasurface design. Having a diversity of device layouts for a given optical function is also practically useful in experimental implementation, to account for any constraints in the fabrication process. For this analysis, we estimate the computational time required to produce "above threshold" devices, previously defined for vetting the training set earlier, across the full parameter space featured in Figure 3a.

The results are summarized in Figure 4a and Table S2. For devices designed using brute force optimization, only 40% of devices designed from scratch fulfill our high efficiency threshold. The total computation cost scales accordingly as a function of the total number of desired devices (red line). The GAN-based approach requires a large initial computation cost due to the generation of training data. However, the computational cost of designing "above threshold" devices using GAN generation, evaluation, and device refinement is relatively low. The result produces a trend for computational cost described by the blue line, which has a slope approximately three times less steep than that of the red line. The data used for this analysis are taken from a broad range of wavelength and angle pairs and are summarized in Fig. S4. We find that the total computational cost of our GAN-based approach is lower than that of brute-force optimization if we want to design more than ~930 devices, and the advantages in computational cost scale with increasing device numbers. In addition to savings in total computational cost, we also have potential savings in total computation time when using multiple computing cores, due to the enhanced parallelizability of our design approach compared to the brute force approach.

Finally, we show that the capabilities of our conditional GAN can be enhanced by network retraining with additional data. These data can originate from two sources. The first is from brute force optimization, which is how we produced our initial metagrating training set. The second is from the GAN generator and iterative optimizer themselves, which yield high efficiency devices. This second source of training data suggests a pathway to expanding the efficacy of our conditional GAN with high computational efficiency.

As a proof-of-concept, we use the generator and iterative optimizer to produce 6000 additional high efficiency (70%+) robust metagratings with wavelengths and angles spanning the full parameter space featured in Fig. 3a. We then add these data to our previous training set and retrain our conditional GAN. Fig. 4b shows the device efficiencies from the retrained generator, where 5000 devices for a given angle and wavelength are generated and the efficiencies of the highest performing devices are presented. The plot shows that the efficiency values of devices produced by the retrained GAN generally increase in comparison to those produced by the original GAN. Quantitatively, over 80% of the devices in the parameter space have improved efficiencies after retraining (Fig. 4c). We attribute the efficiency reduction of the remaining devices to a suboptimal

selection of hyperparameters and network architecture, which require tuning upon each retraining step. An examination of the efficiency histograms of devices produced by the initial and retrained GAN, for the device parameters featured in Fig. 2, show that the retrained GAN produces devices with average and maximum efficiencies approximately 10% higher than those form the initial GAN. As such, the retrained GAN has learned to generate better devices. An understanding of how to systematically refine the conditional GAN architecture and hyperparameters upon retraining will be the subject of future work.

A schematic of our overall design platform is presented in Fig. 5. To produce metagratings with a desired set of device parameters, we first use the conditional GAN to generate many candidate device images, with a diversity of geometric shapes made possible by the random number array input. These devices are characterized using a high-speed electromagnetics simulator, and we filter for devices that have high efficiencies. We then use optimization to refine these patterns and incorporate experimental constraints and robustness into the designs. These final metagrating layouts serve as new training data to retrain the conditional GAN and expand its overall capabilities. This method of GAN refinement can be performed iteratively in an automated manner, where the input device parameters are specified to be near but not overlapping with those in the training set, and the output devices are used for network retraining.

In summary, we show that generative neural networks can facilitate the computationally efficient design of high performance, topologically-complex metasurfaces in cases where it is of interest to generate a large family of designs. Neural networks are a powerful and appropriate tool for this design problem for two reasons. First, there exists a strong interdependence between device topology and optical response, particularly for high performance devices. Second, we have the capability to generate high quality training data and validate device performance using the combination of iterative optimizers and accurate electromagnetic solvers.

While this study focuses on the variation of two device parameters (i.e., wavelength and deflection angle), one can imagine generalizing the GAN-based approach to other device parameters, such as device thickness, device dielectric, polarization, phase response, and incidence angle. With a higher dimensional parameter space, brute force optimization methods simply cannot scale, making data-driven methods a necessary route to the design of topologically-complex devices. The scaling of our methods to higher dimensional parameter spaces will require particular attention paid to the proper selection of training set parameters, vetting of the network architecture, and metrics for evaluating the efficacy of the generative network. If successful, such generative networks could serve as a means to producing truly large datasets of topologically-optimal metasurfaces, paving the way for the use of other big data machine learning schemes for device analysis and discovery.

We envision that data-driven design processes will apply to the design and characterization of other complex nanophotonic devices, ranging from dielectric and plasmonic antennas to photonic crystals. The methods we described will broadly encompass the design of devices and structured materials in other fields, such as acoustics, mechanics, and electronics, where there exist strong relationships between structure and response.

Acknowledgments: The simulations were performed in the Sherlock computing cluster at Stanford University. **Funding:** This work was supported by the U.S. Air Force under Award Number FA9550-18-1-0070, the Office of Naval Research under Award Number N00014-16-1-2630, and the David and Lucile Packard Foundation. DS was supported by the National Science Foundation (NSF) through the NSF Graduate Research Fellowship. **Competing interests:** Authors declare no competing interests.

References and Notes:

1. N. Yu, F. Capasso, Flat optics with designer metasurfaces. *Nature Materials* **13**, 139-150 (2014).
2. A. V. Kildishev, A. Boltasseva, V. M. Shalaev, Planar Photonics with Metasurfaces. *Science* **339**, 1232009 (2013).
3. A. I. Kuznetsov, A. E. Miroshnichenko, M. L. Brongersma, Y. S. Kivshar, B. Luk'yanchuk, Optically resonant dielectric nanostructures. *Science* **354**, aag2472 (2016).
4. M. Khorasaninejad, F. Capasso, Metalenses: Versatile multifunctional photonic components. *Science* **358**, eaam8100 (2017).
5. R. C. Devlin, A. Ambrosio, N. A. Rubin, J. P. B. Mueller, F. Capasso, Arbitrary spin-to-orbital angular momentum conversion of light. *Science* **358**, 896-901 (2017).
6. A. Tittl, A. Leitis, M. Liu, F. Yesilkoy, D.-Y. Choi, D. N. Neshev, Y. S. Kivshar, H. Altug, Imaging-based molecular barcoding with pixelated dielectric metasurfaces. *Science* **360**, 1105-1109 (2018).
7. G. Zheng, H. Mühlenbernd, M. Kenney, G. Li, T. Zentgraf, S. Zhang, Metasurface holograms reaching 80% efficiency. *Nature Nanotechnology* **10**, 308-312 (2015).
8. J. B. Pendry, A. Aubry, D. R. Smith, S. A. Maier, Transformation Optics and Subwavelength Control of Light. *Science* **337**, 549-552 (2012).
9. A. Silva, F. Monticone, G. Castaldi, V. Galdi, A. Alù, N. Engheta, Performing Mathematical Operations with Metamaterials. *Science* **343**, 160-163 (2014).
10. N. Yu, P. Genevet, M. A. Kats, F. Aieta, J.-P. Tetienne, F. Capasso, Z. Gaburro, Light Propagation with Phase Discontinuities: Generalized Laws of Reflection and Refraction. *Science* **334**, 333-337 (2011).
11. A. Arbabi, Y. Horie, M. Bagheri, A. Faraon, Dielectric metasurfaces for complete control of phase and polarization with subwavelength spatial resolution and high transmission. *Nature Nanotechnology* **10**, 937 (2015).
12. M. Khorasaninejad, W. T. Chen, R. C. Devlin, J. Oh, A. Y. Zhu, F. Capasso, Metalenses at visible wavelengths: Diffraction-limited focusing and subwavelength resolution imaging. *Science* **352**, 1190-1194 (2016).
13. M. Decker, I. Staude, M. Falkner, J. Dominguez, D. N. Neshev, I. Brener, T. Pertsch, Y. S. Kivshar, High-Efficiency Dielectric Huygens' Surfaces. *Advanced Optical Materials* **3**, 813-820 (2015).

14. J. S. Jensen, O. Sigmund, Topology optimization for nano-photonics. *Laser & Photonics Reviews* **5**, 308-321 (2011).

15. A. Y. Piggott, J. Lu, K. G. Lagoudakis, J. Petykiewicz, T. M. Babinec, J. Vučković, Inverse design and demonstration of a compact and broadband on-chip wavelength demultiplexer. *Nature Photonics* **9**, 374 (2015).

16. D. Sell, J. Yang, S. Doshay, K. Zhang, J. A. Fan, Visible Light Metasurfaces Based on Single-Crystal Silicon. *ACS Photonics* **3**, 1919-1925 (2016).

17. Z. Lin, B. Groever, F. Capasso, A. W. Rodriguez, and M. Lončar, Topology-Optimized Multilayered Metaoptics. *Physical Review Applied*, **9**(4), p.044030 (2018).

18. T. P. Xiao, O. S. Cifci, S. Bhargava, H. Chen, T. Gissibl, W. Zhou, H. Giessen, K. C. Toussaint Jr, E. Yablonovitch and P. V. Braun, Diffractive Spectral-Splitting Optical Element Designed by Adjoint-Based Electromagnetic Optimization and Fabricated by Femtosecond 3D Direct Laser Writing. *ACS Photonics*, **3**(5), pp.886-894 (2016).

19. D. Sell, J. Yang, S. Doshay, J. A. Fan, Periodic Dielectric Metasurfaces with High-Efficiency, Multiwavelength Functionalities. *Advanced Optical Materials* **5**, 1700645 (2017).

20. J. Yang, J. A. Fan, Topology-optimized metasurfaces: impact of initial geometric layout. *Opt. Lett.* **42**, 3161-3164 (2017).

21. I. J. Goodfellow, J. Pouget-Abadie, M. Mirza, B. Xu, D. Warde-Farley, S. Ozair, A. Courville, Y. Bengio, paper presented at the Proceedings of the 27th International Conference on Neural Information Processing Systems - Volume 2, Montreal, Canada, 2014.

22. M. Mirza, Z. Osindero, Conditional Generative Adversarial Nets. *arXiv:1411.1784*, (2014).

23. D. Sell, J. Yang, S. Doshay, R. Yang, J. A. Fan, Large-Angle, Multifunctional Metagratings Based on Freeform Multimode Geometries. *Nano Letters* **17**, 3752-3757 (2017).

24. J. Yang, D. Sell, J. A. Fan, Freeform Metagratings Based on Complex Light Scattering Dynamics for Extreme, High Efficiency Beam Steering. *Annalen der Physik*, 1700302 (2017).

25. J. Peurifoy, Y. Shen, L. Jing, Y. Yang, F. Cano-Renteria, B. G. DeLacy, J. D. Joannopoulos, M. Tegmark, M. Soljačić, Nanophotonic particle simulation and inverse design using artificial neural networks. *Science Advances* **4**, eaar4206 (2018).

26. W. Ma, F. Cheng, Y. Liu, Deep-Learning-Enabled On-Demand Design of Chiral Metamaterials. *ACS Nano* **12**, 6326-6334 (2018).

27. D. Liu, Y. Tan, E. Khoram, Z. Yu, Training Deep Neural Networks for the Inverse Design of Nanophotonic Structures. *ACS Photonics* **5**, 1365-1369 (2018).

28. S. Inampudi, H. Mosallaei, Neural network based design of metagratings. *Applied Physics Letters* **112**, 241102 (2018).

29. I. Malkiel, M. Mrejen, A. Nagler, U. Arieli, L. Wolf, H. Suchowski, Plasmonic nanostructure design and characterization via Deep Learning. *Light: Science & Applications* **7**, 60 (2018).

30. F. Wang, J. S. Jensen, O. Sigmund, Robust topology optimization of photonic crystal waveguides with tailored dispersion properties. *J. Opt. Soc. Am. B* **28**, 387-397 (2011).

31. J. P. Hugonin, P. Lalanne, Reticolo software for grating analysis, Institut d'Optique, Orsay, France. (2005).

32. J. Yang, J. A. Fan, Analysis of material selection on dielectric metasurface performance. *Opt. Express* **25**, 23899-23909 (2017).

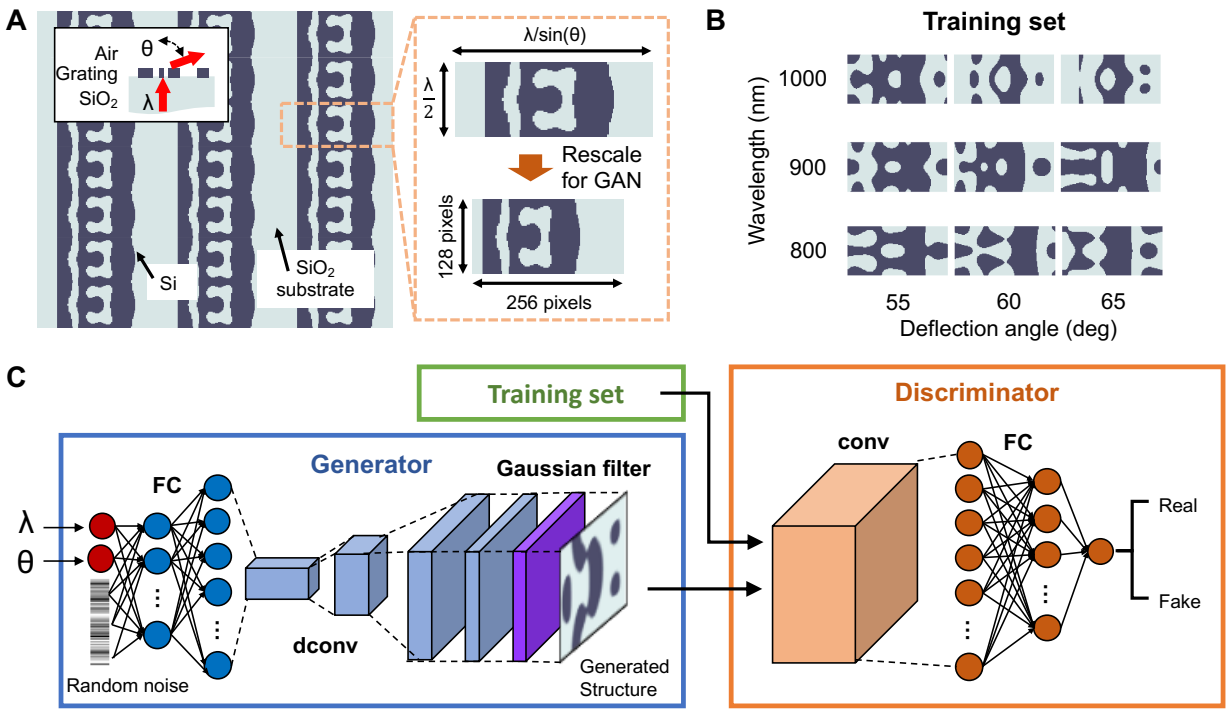

Fig. 1. Machine learning with topology-optimized metagratings. (A) Top view image of a typical topology-optimized metagrating that selectively deflects light to the +1 diffraction order. The input data to the GAN are images of single metagrating unit cells rescaled to a 128 x 256 pixel grid. (B) Representative images of metagratings in the training set. All devices deflect TE-polarized light with over 75% efficiency, and each is designed to operate for a specific deflection angle and wavelength. (C) Schematic of the conditional GAN for metagrating generation. The generator utilizes two fully connected (FC) and four deconvolution (dconv) layers, followed by a Gaussian filtering layer, while the discriminator utilizes one convolutional (conv) layer and two fully connected layers. After training, the generator produces images of new, topologically-complex devices designed for a desired deflection angle and wavelength.

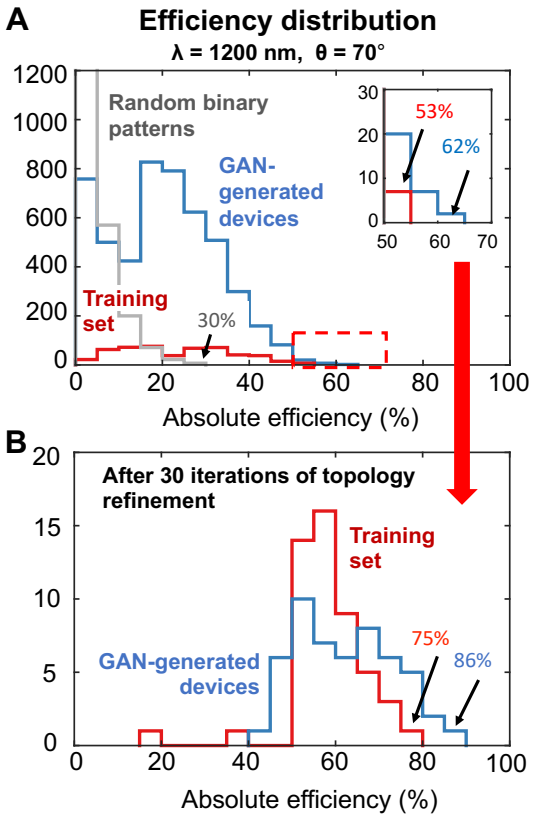

Fig. 2. Metagrating generation and refinement. (A) Efficiency histograms of metagratings produced from the trained GAN generator, training set, and randomly generated binary patterns. The design wavelength and angle for these devices are 1200 nm and 70 degrees, respectively. The highest device efficiencies in the histograms are displayed. Inset: Magnified view of the histogram outlined by the dashed red box. (B) Efficiency histogram of metagratings from the trained GAN generator and training set, refined by topology optimization. The 50 highest efficiency devices from the GAN generator and training set are considered for topology refinement. The highest efficiency devices produced from the training set and GAN generator are displayed.

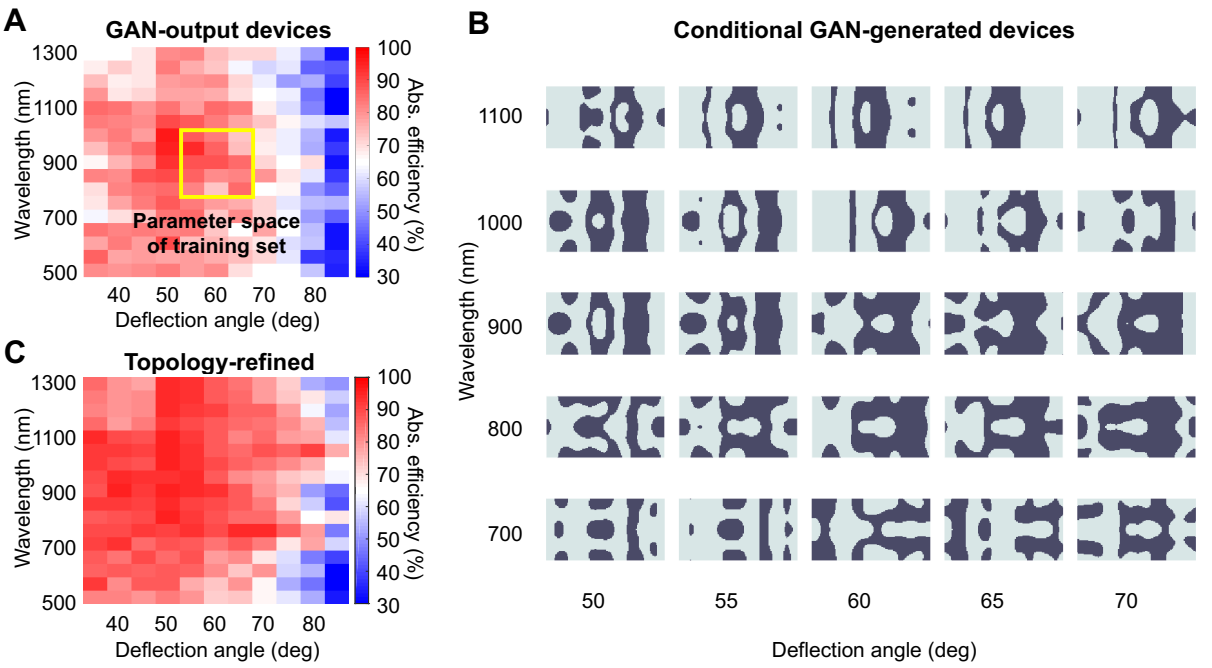

Fig. 3. Metagrating performance across a broad parameter space. (A) Plot of the highest device efficiencies for metagratings produced by the GAN generator for differing wavelength and deflection angle parameters. The solid yellow box represents the range of parameters covered by devices in the training set. (B) Representative images of high efficiency metagratings produced by the GAN generator for differing operating wavelengths and angles. (C) Plot of the highest device efficiencies for metagratings generated from the conditional GAN and then topology-optimized.

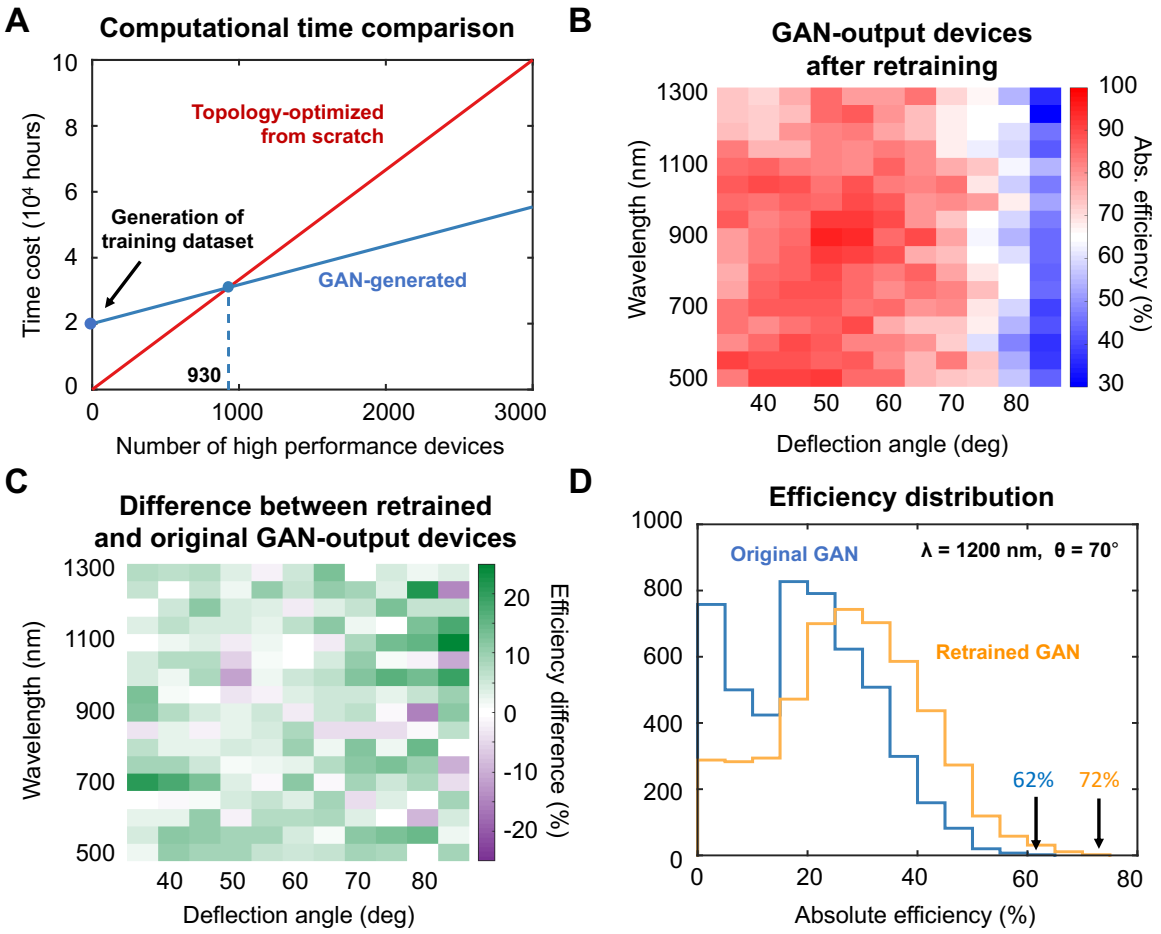

Fig. 4. Benchmarking of GAN-based computational cost and network retraining efficacy. (A) Time cost of generating ***n*** "above threshold" devices using topology optimization from scratch (red line) and GAN-generation and refinement (blue line). The offset of the blue line is from the computational cost of generating the training set. "Above threshold" is defined in the main text. (B) Plot of the highest device efficiencies for metagratings produced by a retrained GAN generator. The initial training set is supplemented with an additional 6000 high efficiency devices operating across the entire parameter space. (C) Plot of differences in device efficiencies between those produced by the retrained GAN generator in (B) and those produced by the initial GAN generator in Fig. 3a. (D) Efficiency histogram of metagratings produced by the initial and retrained GAN, for operating parameters matching those in Fig. 2. With more training data, the devices produced by the retrained GAN have on average 10% higher efficiencies, and the highest efficiency device also is boosted in performance.

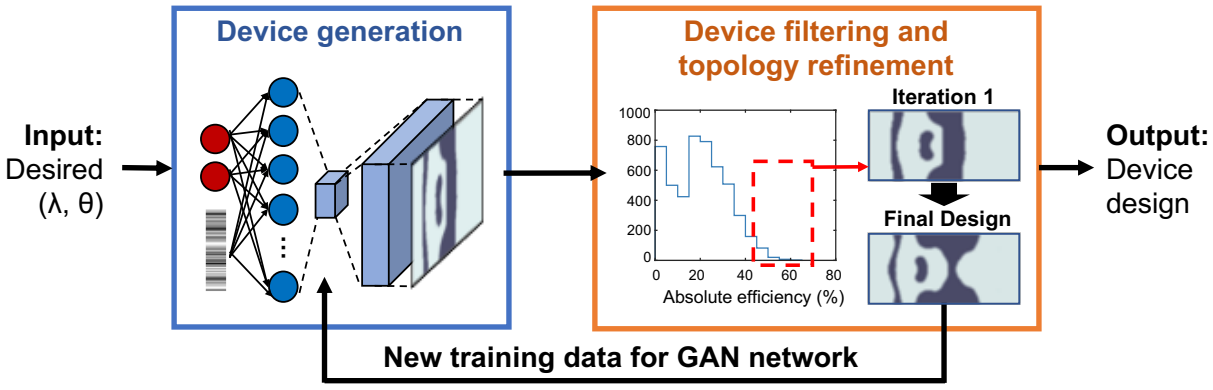

Fig. 5. Schematic of metasurface inverse design based on device generation from a conditional GAN generator, followed by topology optimization. Devices produced in this manner can be fed back into the conditional GAN for retraining and network refinement**.**